Comparison of pressure surge events in water and liquid nitrogen as a substitute fluid for rocket engine feed lines

Sebastian Klein, Tobias Traudt, Prof. Michael Oschwald

German Aerospace Center | Institute of Space Propulsion | Rocket Propulsion

Abstract

Testing transient phenomena in space propulsion systems is very complex due to propellants being reactive and often cryogenic. The use of non-reactive replacement fluids lowers the risk and therefore the effort of testing. A common replacement fluid is water, which is easy to handle and widely accessible. This paper aims for the comparison between water and liquid nitrogen (LN2) as a cryogenic replacement fluid. Several fluid hammer tests with both fluids were performed at the Fluid Transient Test Facility (FTTF) at DLR Lampoldshausen. Seven test cases with LN2 are presented in detail. At high pressure levels, there is good agreement with the predicted Joukowsky pressure rise and fluid hammer eigenfrequencies. Furthermore, a systematically interruption of the first pressure rise was observed. By comparing LN2 and water experiments, it was found that higher eigenmodes of the fluid hammer occurred after cavitation only in water experiments.

1 INTRODUCTION

Fluid hammer is an important parameter in the process of liquid rocket engines. To reach orbit with high payload mass, it is important that engines and piping system are as lightweight as possible. Nevertheless, the engines must operate reliable, since a failure would lead to the loss of the rocket. A well-known example is the loss of the 4th flight of the N1-L3 soviet lunar rocket. After shut down of an engine, a shock wave destroyed an oxygen pump [1]. Fluid hammer in space environment is not limited to rocket engines, it is also a challenge in the design process of spacecrafts. In satellites fluid hammer can occur in the propellant circuit, therefore tests with Mono Methyl Hydrazine and Nitrogen Tetroxide were performed by Gibek & Maisonneuve [2]. While testing the automated transfer vehicle (ATV) with water as a substitute fluid, pressures up to 220 bar were measured, which exceeded the specifications [3]. Due to its easy access and inert properties it is common to use water as a substitute fluid. Several rocket engines are operated with cryogenic propellants [4]. Liquid hydrogen and liquid oxygen are used in the main and upper stage of the Ariane 6 rocket. Since these fluids are reactive and water is not cryogenic, there is a need of fluid hammer experiments with an inert, cryogenic fluid. These requirements are fulfilled by liquid nitrogen (LN2). Priming experiments with LN2 were conducted and compared to simulation by Gouriet *et al.* [5]. However, there is currently limited research on the phenomenon of fluid hammer in LN2,

particularly with regards to the pressure surge triggered by the stopping of a stationary flow.

The **F**ast **T**ransient **T**est **F**acility (**FTTF**) at DLR Lampoldshausen is used to investigate fluid hammer experiments with water and LN2. To identify differences and similarities between fluids, experiments were conducted first with water due to its well-known behavior, followed by comparable experiments with LN2. Several topics, including but not limited to water hammer wave shape [6], high speed imaging of water hammer [7], the influence from cavitation on the acoustic boundary conditions [8] and cavitation induced noise growth in water and LN2 [9], were studied in detail. Reference [10] provides a comprehensive analysis comparing water and LN2 fluid hammer, emphasizing the first cavitation valley and its duration.

This work focuses on the description of LN2 fluid hammer events with the occurrence of cavitation. Several test cases with changing initial conditions will be presented. The experimental data then will be evaluated by comparing them with the analytical solution of the Joukowsky pressure rise and the fluid hammer eigenfrequency. The influence of the initial conditions on the pressure wave shape will be discussed. Finally, fluid hammer is compared in LN2 and water. 1

2 THEORY

The pressure rise during a pressure surge event can be calculated with the Joukowsky equation [11].

$$\Delta P_J = -\rho a \Delta v \tag{1}$$

Where ΔP_J is the magnitude of the pressure surge caused by the velocity change Δv. For cases where the valve is fully closed completely, $\Delta v = -v_0$, where v_0 is the initial flow velocity before valve closure. The density ρ is a fluid property, the speed of sound a in an elastic pipeline differs from the speed of sound in the fluid itself. It was first derived by Korteweg [12].

$$\mathrm{a} = \sqrt{\frac{K/\rho}{1 + \left(\frac{K}{E}\right)\left(\frac{D}{e}\right) c_1}} \tag{2}$$

Where K is the fluids bulk modulus, E is the Young modulus of the pipe, D is the inner diameter of the pipe and e is the wall thickness. The factor c_1 for thick walled pipes ($D/e > 25$) which are anchored against longitudinal movement is a function of the pipe's geometry and the Poisson coefficient ν [13]:

$$\mathrm{c}_1 = \frac{2e}{D}(1 + \nu) + \frac{D(1 - \nu^2)}{D + e} \tag{3}$$

After valve closure, a compression wave travels through the pipeline of length l with the wave speed a until it reaches the valve. The pressure rise over the wave front is given by

ΔP_J, due to the compressibility of the fluid, the density increases behind the wave front. After being reflected at the valve, the wave travels back towards the pipe. The pressure behind the wave front equals the initial pressure. The wave is then reflected at the valve and travels as a rarefaction wave towards the reservoir and back. Here it is reflected again and is changed back to a compression wave. This process requires the wave to travel four times towards the pipe, therefore the frequency f is:

$$f = \frac{a}{4l} \tag{4}$$

This is the same equation as for calculation of a standing wave in a tube open at one end and closed at the other. The different eigenmodes can be calculated by adding a pre-factor dependent to the mode number n to equation **4**. This results in equation **5**:

$$f(n) = (2n - 1) \cdot \frac{a}{4l} \tag{5}$$

If the amplitude of the pressure surge is so big, that die rarefaction wave undershoots the vapor pressure of the fluid, cavitation forms near the valve. Unlike fluid hammer without cavitation, the velocity behind the pressure wave v_1 is not reduced to zero but to:

$$v_1 = v_0 - \frac{P_0 - P_V}{\rho a} \tag{6}$$

In a horizontal pipe an area of concentrated cavitation at the valve with distributed cavitation in the pipeline is expected [14]. It is worth noting that the duration of this cavitation exceeds the period of the fluid hammer. A simple model to estimate the cavitation duration Δt_c is given by Reference [15]:

$$\Delta t_c = A_{rel} \cdot \frac{2l}{a} = \frac{P_1 - P_0}{P_0 - P_V} \cdot \frac{2l}{a} \tag{7}$$

Where A_{rel} is the relative amplitude, which is the ratio between the difference of the peak pressure P_1 and the initial pressure P_0 and the difference between P_0 and the vapor pressure of the fluid P_V. Another way to calculate Δt_c is to solve the differential equations **8** and **9** (Prasser Model):

$$\rho \cdot l \cdot \frac{\mathrm{dv}}{\mathrm{dt}} = P_V - P_G - \Delta P_{ges} \tag{8}$$

and

$$x_c = \int_0^t v \cdot dt \tag{9}$$

Where P_G is the backpressure of the tank, ΔP_{ges} is the pressure loss in the system and t is the time. The movement of the liquid column is calculated by considering the inertia of the liquid column and the pressure force P_G pushing from one side and P_V pulling from the other [16]. This model assumes a perfect separation between gas and liquid column, which is not necessarily true in reality. It was found that the Prasser model showed

significantly better agreement with experimental data generated on the test bench used in this work [10]. The speed of sound in a two-phase flow a_{2p} decreases significantly compared to single-phase flow. This can be calculated by the Wood equation, where the subscripts $\cdot_g$ and $\cdot_l$ indicates gaseous and liquid phases, and χ is the void fraction [17].

$$\frac{1}{a_{2p}^2} = \frac{(1-\chi)^2}{a_l^2} + \frac{\chi^2}{a_g^2} + \chi(1-\chi)\frac{\rho_g^2 a_g^2 + \rho_l^2 a_l^2}{\rho_l \rho_g a_l^2 a_g^2} \qquad 10$$

3 FAST TRANSIENT TEST FACILITY

Two configurations of the FTTF were used to perform fluid hammer experiments. Since the water configuration (FTTF-1) is well described by Traudt et al. [7]. This work is focusing on the LN2 configuration (FTTF-2).

3.1 Test bench

The FTTF-2 is a test bench with changeable test sections to investigate the phenomenon of cryogenic pressure surges. A schematic of the test bench is shown in Figure 1Figure 1: Schematic of the liquid nitrogen fluid hammer test bench.. The test bench itself contains two identical tanks, which can be pressurized with gaseous nitrogen. The Coriolis flow meter, type EMRSON CMF50M, and the pneumatically operated axial valve are both surrounded by foam isolated to avoid heat entrance from the environment. The valve has a closing time of approximately $t_{valve} = 18$ ms.

The test section is a pipeline with a one and a half upward $(0.62°)$ spiral, which is wrapped in a vacuum jacket. It contains three sensor positions where pressure and temperature are measured. In this paper the first position is the most important one. The temperature is measured using a thermocouple type K (sampling rate: 100 Hz), while the pressure is measured with a Kulite CTL-190S-2000A at a sampling rate of 10 kHz. The pressure measurement is flush-mounted, whereas the temperature sensor is inserted into the flow where it measures at the center of the cross section. Test bench and test section are made of stainless-steel grade 1.456.

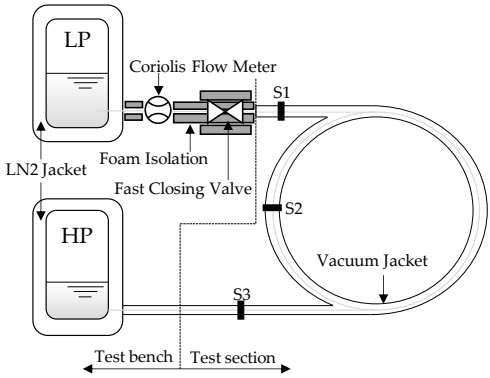

Figure 1: Schematic of the liquid nitrogen fluid hammer test bench.

The water configuration is basically the same test bench without any kind of isolation, since water hammer experiments were performed at ambient temperature. Most important geometry differences between both configurations are given in Table 1.

Table 1: Dimensions of the test bench

Description	Symbol	Water	LN2
Test section length	l_{ts}	7.671 m	9.29 m
Test section inner pipe diameter	$D_{i,ts}$	19 mm	19 mm
Test section wall thickness	e_{ts}	1.5 mm	1.5 mm
Sensor position 1 (from valve seat)	l_1/l_{ts}	3.9 %	6.46 %

3.2 Procedure

Before testing, the whole test bench and test section must be cooled down. After the cooling process, fluid is moved into the HP tank and the valve is closed. The filling level of the LP tank remains as high that the tank outlet is fully covered with LN2. The HP Tank is then pressurized to a desired pressure. Next the valve is opened for 10 s so that a steady flow can be established. This long period of flow also helps achieving a constant fluid temperature. The valve is then closed and a fluid hammer wave is measured in the test section. After each test, liquid nitrogen is pushed back into the HP tank. The constant moving of the fluid between tests reduces the temperature of the test bench.

4 RESULTS

The experimental results are presented in this section. Seven test cases with liquid nitrogen are described in detail and compared to analytical solutions. In the following, these results will be compared with water hammer data from the same test bench.

4.1 Nomenclature

The nomenclature used in this paper is illustrated in Figure 2 as an example based on the pressure curves of test case 7. The initial pressure and temperature are given by index $\cdot_0$. The conditions of the fluid in the following pressure peaks are marked by indices $\cdot_1; \cdot_2; \ldots \cdot_n$, consequently the indices in the pressure valleys are: $\cdot_{1'}; \cdot_{2'}; \ldots \cdot_{n'}$. The pressure increase from the initial pressure towards the peak pressures is given by: $\Delta P_n = P_n - P_0$, the pressure decrease in the valleys is $\Delta P_{n'} = \Delta P_{n'} - P_0$.

The pressure traces in Figure 2 show a typical fluid hammer in liquid nitrogen. After the valve closure, a pressure wave travels towards the system and the maximum pressure P_1 is reached in the first peak. Cavitation occurs in the first three valleys, detected by constant pressure ($P_{1'}; P_{2'};\ P_{3'}$) close to the vapor pressure of the fluid. Furthermore, the pressure amplitudes $\Delta P_1;\ \Delta P_2;\ \Delta P_3$ are much bigger than their counterparts $|\Delta P_{1'}|;\ |\Delta P_{2'}|; |\Delta P_{3'}|$. Pressure peaks 2-4 are very similar in height, one possible

explanation is the superposition of the fluid hammer and a pressure wave triggered by the collapse of cavitation. This is a well-known phenomenon and described for example in reference [14]. After the last valley with occurrence of cavitation, a damped harmonic oscillation is established.

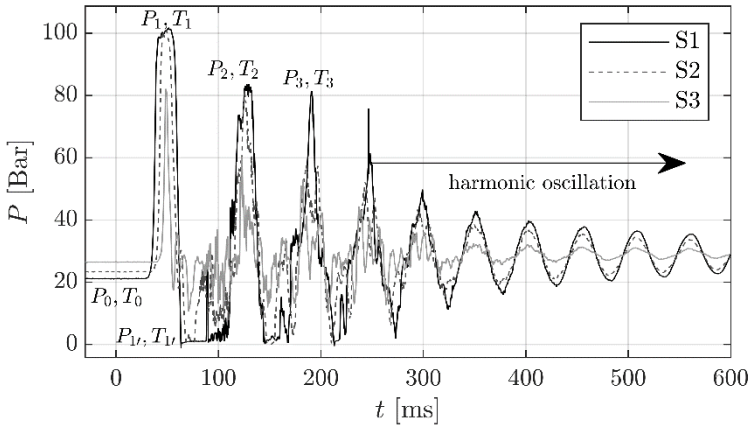

Figure 2: LN2: Nomenclature used in this work is given by the pressure traces of test case 7 at all three sensor positions.

4.2 LN2: Test cases

Seven test cases (TC1 – TC7) with different initial tank pressures are presented in this chapter. All tests were performed on the same day within several hours, since the test bench is indoors, the environmental temperature is considered equal for all test cases (~293 K). The initial tank pressures P_{HP} and P_{LP} are given in Figure 3. To achieve high flow velocities, the LP tank was left open. Since the tanks are secured against the ingress of air with a check valve, the pressure in the LP tank is slightly above atmospheric pressure.

The pressure in the HP Tank P_{HP} increases from 1.84 bar (test case 1) to 28.05 bar (test case 7). The flow velocity increases with higher pressure difference between both tanks, consequently the fluid hammer pressure rises from 17 bar in test case 1 up to over 100 bar in test case 7.

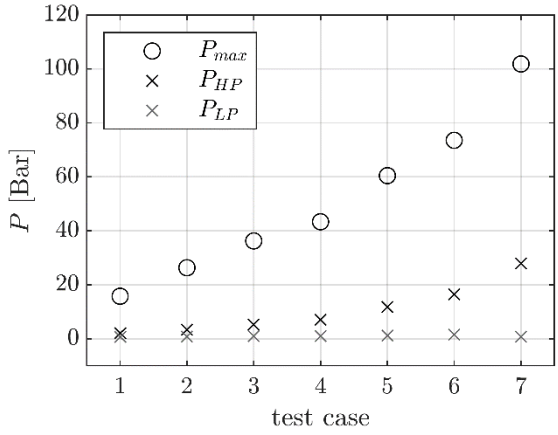

Figure 3: LN2 test case overview, HP- and LP-Tank pressure before valve closing: $\boldsymbol{P_{HP}}$, $\boldsymbol{P_{LP}}$; maximum measured pressure while the event of a fluid hammer $\boldsymbol{P_{max}}$

In Figure 4 pressure traces at sensor position S1 for all seven test cases are shown. A first pressure peak is visible in all test cases. The second pressure peak is slightly visible in test case 2 and clearly observable thereafter. Cavitation after the first peak is visible from case 3 onwards. It is not clearly observable in test case 1 and 2, therefore it will not be considered in detail in the following. The duration of the cavitation decreases for higher test cases.

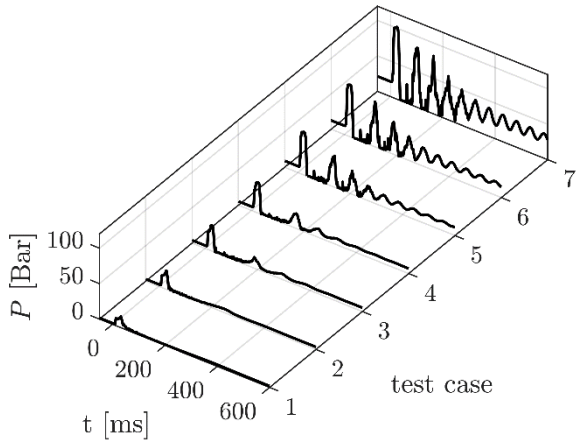

Figure 4: LN2: Pressure traces at sensor at position S1 for different initial conditions, shown in **Figure 3**

In addition to the pressure traces in Figure 4, temperature readings at the same location are given in Figure 5. The temperature at $t_0 = 0$ s is approximately $T_{0,TC1..5} = 85.5 \pm 0.5$ K in the first five test cases. It is slightly higher in test case 6, $T_{0,TC6} = 86.4$ K and

even higher in test case 7, $T_{0,TC7}(t_0) = 87.1$ K. The tanks are cooled by the LN2 jackets, where nitrogen boils at approximately atmospheric pressure but the vacuum and foam isolated parts receive heat input. Since it takes some time to pressurize the testbench, it is not depressurized to atmospheric pressure between the individual tests. As a consequence, liquid nitrogen in the test section can heat up to higher temperatures without boiling, this effect is assumed to be the reason for the higher temperatures in test case 6 and 7.

The fluid hammer detected in Figure 4 can also be found in temperature readings in Figure 5. The first peak can be identified from the third test case onwards. The rise in temperature increases with increasing maximum pressure. In test case 6 and 7 even several temperature peaks can be detected. The maximum temperature recorded can be found in test case 7 while the initial fluid hammer wave $T_1 = 89.4$ K, this corresponds to a temperature rise $\Delta T_1 = T_1 - T_0 = 2.6$ K. In test case 7, a temperature drop during the first cavitation valley can also be observed. A minimum temperature of $T_{1'} = 86.3$ K leads to $\Delta T_{1'} = T_{1'} - T_0 = -0.8$ K. The most likely cause for the temperature dynamics are the effects of compression and expansion.

Since the temperature is measured with a thermocouple it is suspected, that the measurement does not fully cover the transient behavior of the temperature. As shown in reference [18] thermocouples are relatively slow compared to infrared highspeed temperature measurement.

In test cases 1 and 3 some temperature changes after approximately 250 ms are visible, the reason for this phenomenon is unclear and will not investigated further in this work.

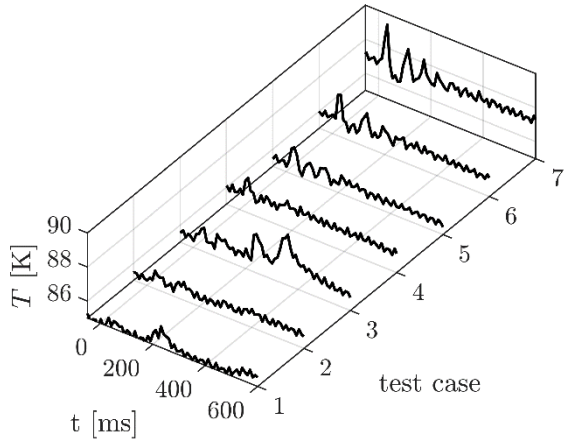

Figure 5: LN2: Temperature traces at sensor at position S1 for different initial conditions, shown in **Figure 3**

In Figure 6 the ratio of P_0 to P_V as well as A_{rel} are shown over P_0. While P_0 increases with each test case, P_V remains nearly constant, since T_0 varies only a few Kelvin. The minimal vapor pressure was calculated at TC1 for $P_{V,TC1}(T_{0,TC1}) = 2.29$ bar, while the maximum vapor pressure was determined in TC2 with a value of $P_{V,TC7}(T_{0,TC7}) =$

2.77 bar. In TC1 P_0 is smaller than P_V, which suggests a gaseous flow. This is also the reason for the negative A_{rel} in TC1. However, the density measurement in the Coriolis flow meter of $\rho_0 = 779.2^{+2.88}_{-1.06}$ kg/m³ indicates a liquid flow in all test cases. Except from TC1, A_{rel} decreases across all test cases, resulting in shorter cavitation duration. This goes along with the observations in Figure 4.

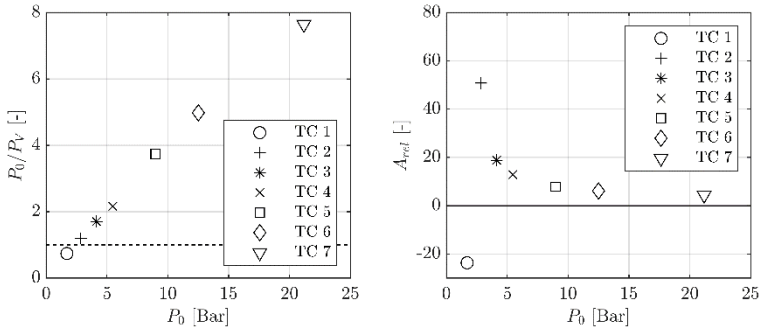

Figure 6: Ratio of initial pressure $\boldsymbol{P_0}$ to vapor pressure $\boldsymbol{P_V}$ and relative Amplitude $\boldsymbol{A_{rel}}$

4.3 LN2: Comparison with analytical solution

The amplitude of the first pressure peak ΔP_1 is compared to the Joukowsky pressure rise (equation **1**), the results are plotted in Figure 7. On the experimental side, ΔP_1 is selected by taking the maximum pressure of the first peak. To calculate ΔP_J, ρ, T and $\dot{m}$ are measured by the Coriolis flow meter. The last data point before valve closure is taken. Then, the flow velocity is calculated using these parameters and the geometry of the pipeline. The pressure ratio $\Delta P_1/\Delta P_J$ is plotted over the initial pressure before valve closing P_0.

In test case 1 only 78% of the Joukowsky pressure rise is reached. In test case 2 the matching ratio is over 90%, further test cases show a matching over 96%. Test case 7 slightly overshoots the prediction by Joukowsky (102 %). Since all test cases were performed at comparable temperatures, it is most likely that the better matching is caused by higher pressure. A possible explanation is the existence of vapor in the flow which dampens the pressure rise. As previously mentioned, the density measurement suggested a liquid flow in all of the test cases. However, it is important to note that the measurement method may not be able to detect a small void fraction, and even a minor amount of gas can significantly reduce the speed of sound (see equation **10**).

To investigate this hypothesis, the first pressure peak is studied in detail. The normalization

$$\mathrm{P_{norm}} = \frac{P - P_0}{P_1 - P_0} \qquad 11$$

is used to achieve a better comparison between individual test cases. In Figure 8 all normalized first peaks are presented. Even though the valve is activated at the same time, the real valve movement differs a couple of milliseconds in each test case. Therefore, the pressure curves are shifted about that time, as if the valve always moved at the same time.

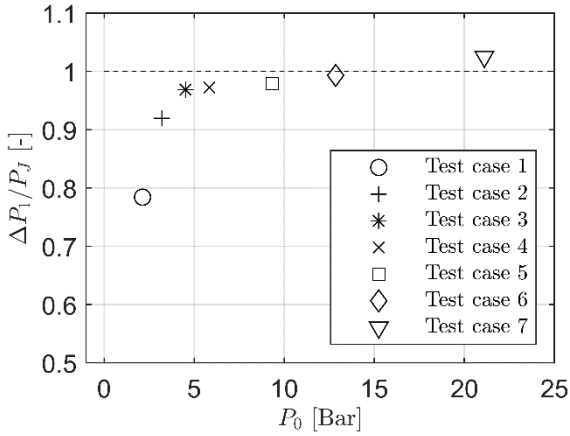

Figure 7: Comparison of experimental measured pressure rise $\boldsymbol{\Delta P_1}$ and Joukowsky pressure rise $\boldsymbol{\Delta P_J}$

The pressure peak can be separated into several areas. First, an interesting part is the pressure rise from $P_{norm} = 0$ to $P_{norm} = 0.6$. Test case 1 shows the longest delay between valve closure and pressure rise. This delay reduces with increasing test number and the associated increasing initial pressure and flow velocity. At $P_{norm} = 0.6$ the pressure rise stops in test case 1 – 4 and some high frequency oscillations are visible. The pressure then increases exponentially to the maximum pressure P_1. This pressure rise is systematically faster for higher test cases. In test case 5,6 and 7, the abrupt stop in pressure rise cannot be observed to the same extent. While it can be seen slightly in test case 5 and 6 at $P_{norm} \approx 0.8$, it can not be seen in test case 7. Overall, test case 5, 6 and 7 look similar, it should be emphasized that P_0 varies in these test cases by 11.8 bar. The initial pressure variance in test case 1-4 is only 7.2 bar. This leads to the conclusion, that the transient behavior of the pressure wave is highly pressure or flow velocity sensitive at low pressures or/and slow flow velocities.

A possible explanation for this phenomenon is that the flow contains vapor phase at low pressures. This leads to a reduction of the density and the speed of sound, which results in lower Joukowsky pressure rise. It is suspected that cavitation bubbles will then be compressed or collapsed due to the high pressure. This leads to more mass flow towards the valve, consequently the pressure increases even more. Over time more and more bubbles are compressed and collapsed, this could be an explanation for the exponential pressure rise.

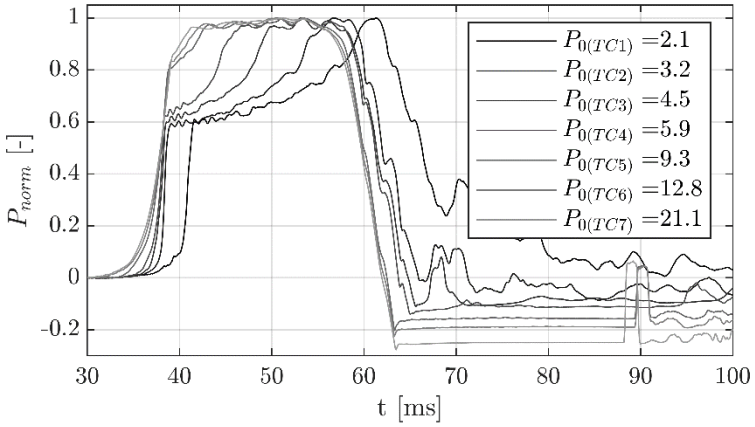

Figure 8: LN2: First pressure peak at Position S1 in multiple test runs with changing initial pressure $\boldsymbol{P_0}$

The pressure wave is damped, consequently there is a point from which cavitation no longer occurs. This point in time is marked in Figure 2. A fast Fourier transformation (FFT) is used in this period to identify the eigenfrequencies of the fluid hammer and compare it with the analytical solutions given in equation **4** and **5**. The results for test case 2 – 7 are plotted in Figure 9. Test case 1 is not considered, since there is no pressure fluctuation after the first peak. The vertical dashed lines mark the calculated eigenfrequencies for the individual test cases. The first eigenmode is around $f(n = 1) =$ 20.5 Hz, consequently the second eigenmode is first one multiplied by three $f(n = 2) =$ 61.5 Hz. Due to small variations in pressure and temperature, the calculated eigenfrequency varies slightly between individual test cases.

In test case 2 and 3 it is not possible to identify an eigenmode via FFT. A broad peak around 13 Hz is visible in test case 4. From the fifth test case on, the first eigenmode can be well identified. The measured eigenmodes are lower than the prediction. The best matching is achieved in test case 7. The second eigenmode is not visible in any test case. The fact that test cases at higher pressures show a better matching supports the theory that there is vapor in low pressure test cases.

4.4 Comparison H2O/ LN2

Test case 7 is compared to a water hammer test case in Figure 10. In the water test case the pressure in the HP tank $P_{HP} = 8.6$ bar. The LP tank is vented, therefore P_{LP} is slightly above ambient pressure, due to the check valve. This setup creates a mass flow of $\dot{m} = 1.78$ kg/s. LN2 and water differ in density and speed of sound. Both are significantly higher in water, this leads to higher Joukowsky pressure rise per flow velocity and higher fluid hammer frequencies. These differences can be observed experimentally. The pressure downstream of the valve (P_{HP}) is equal in both tests. A significantly larger P_{HP} is required to achieve a comparable pressure peak P_1. The dynamics described in Figure 8 were not observed for any pressure in water hammer tests. Since the duration of occurrence of cavitation is coupled to the relative amplitude $A_{rel} = \Delta P_1/P_0$, cavitation in water can be observed over a longer period of time. The pressure rise at the end of the cavitation valleys is very abrupt in water. In LN2 a slow pressure rise at the end of the cavitation valley was observed.

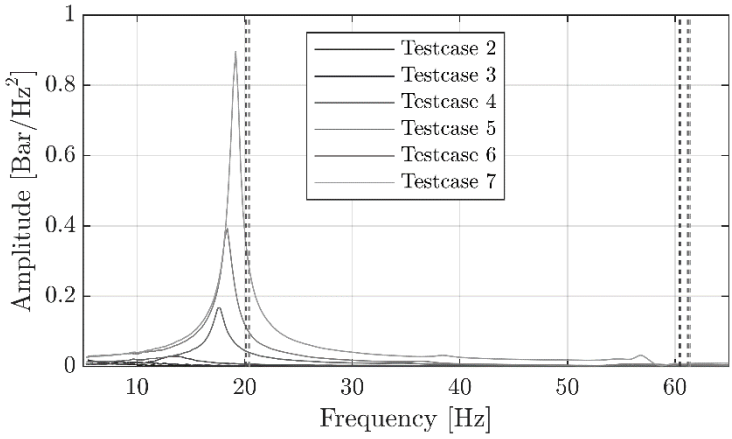

Figure 9: FFT analysis for testcase 2-7. The dashed vertical lines indicate the predicted fluid hammer frequencies.

After the last cavitation valley, the fluid hammer is a damped harmonic oscillation. No higher eigenmodes of the fluid hammer frequency was observer in LN2. In water the higher eigenmodes can be observed from $t = 600$ ms until $t = 800$ ms, as shown in the FFT of the water test case presented in Figure 11. Two peaks are clearly visible, one at 39 Hz, the other at 125 Hz. Both matches well with the calculated eigenfrequencies $f(n)$ for $n = 1$, respectively $n = 2$.

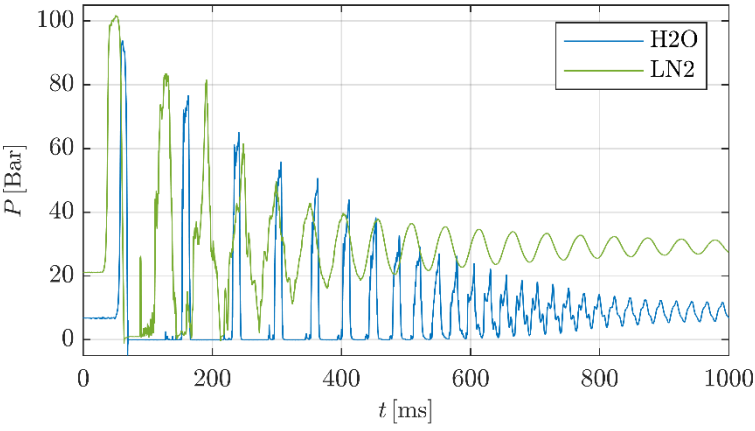

Figure 10: Pressure traces of test case 7 compared with typical water hammer data at sensor position S1.

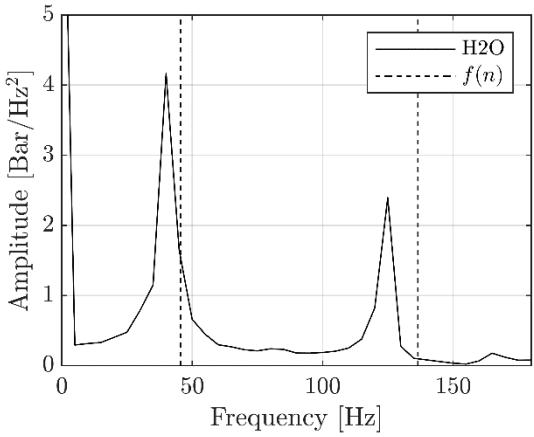

Figure 11: FFT analysis for the water test case from $\boldsymbol{t = 600\ ms}$ to $\boldsymbol{t = 800\ ms}$. The dashed vertical lines indicate the predicted fluid hammer frequencies.

5 CONCLUSION AND OUTLOOK

Fluid hammer tests with liquid nitrogen and water were performed at the FTTF. Seven LN2 test cases with changing initial condition have been described in detail.

- The temperature rise during the initial fluid hammer peak was measured and found to be linked to the pressure amplitude.
- LN2 fluid hammer was compared to analytical solutions. Test cases with an initial pressure over 5 bar showed a good match with the Joukowsky pressure rise. Furthermore, the matching increases with increasing initial pressure.
- The first pressure peak was described in detail, a systematic interruption of the pressure rise was observed. This interruption was found to be more prominent for test cases at lower pressures.
- The frequency of the harmonic oscillation after the cavitation period was compared to the analytical solution. The matching improved at higher pressure levels.
- In comparison with water, the pressure rise at the end of a cavitation valley in LN2 and the occurrence of higher eigenmodes after cavitation in water was found to be the biggest differences between both fluids.

Overall LN2 fluid hammer experiments match well with the analytical prediction at high pressures. The reason for the deviations at low pressure is assumed to be the heat input into the test section and thus the presence of gaseous phase. Therefore, in future experiments the vacuum jacket of the test section will be upgraded to a liquid nitrogen jacket. Furthermore, the fast closing valve will be put into an open liquid nitrogen bath. To get more detailed information about the cavitation dynamics, an optical access will be added next to the valve.

6 REFERENCES

[1] C. Lardier, „The soviet manned lunar program N1-L3,“ *Acta Astronautica,* Bd. 142, pp. 184-192, 2018.

[2] I. Gibek und Y. Maisonneuve, „Waterhammer Tests With Real Propellants,“ in *41st AIAA/ASME/SAE/ASEE Joint Propulsion Conference & Exhibit*, 2005.

[3] V. L'Hullier, „Propulsion in the ATV Spacecraft System-Lessons Learnt,“ in *45th AIAA/ASME/SAE/ASEE Joint Propulsion Conference & Exhibit*, 2009.

[4] O. J. Haidn, „Advanced rocket engines,“ *Advances on propulsion technology for high-speed aircraft,* Bd. 1, p. 6–1, 2008.

[5] J. B. Gouriet, A. Huertas-Martinez, J. M. Buchlin, M. R. Vetrano und J. Steelant, „Multiphase fluid hammer with cryogenic fluids,“ *Proceedings of Space Propulsion 2016,* 2016.

[6] T. Traudt, C. Bombardieri und C. Manfletti, „Influences on Water Hammer Wave Shape an Experimental Study,“ in *63. Deutscher Luft- und Raumfahrtkongress, Augsburg Germany*, 2014.

[7] T. Traudt, C. Bombardieri und C. Manfletti, „High Speed Imaging of Water Hammer with Column Separation,“ in *Pressure Surge Conference, Dublin,* 2015.

[8] S. Klein, T. Traudt und M. Oschwald, „Influence of cavitation on the acoustic boundary conditions in water hammer experiments,“ in *18th International Symposium on Transport Phenomena and Dynamics of Rotating Machinery, ISROMAC,* 2020.

[9] S. Klein, T. Traudt und M. Oschwald, „Comparison between water and liquid nitrogen pressure surge experiments to analyze cavitation induced noise growth,“ in *11th International Symposium on Cavitation*, 2021.

[10] S. Klein, T. Traudt und M. Oschwald, „Comparison of water and cryogenic fluid hammer experiments for rocket engine feed line systems,“ *Experiments in Fluids,* Bd. 64, January 2023.

[11] N. Joukowsky, Über den hydraulischen Stoss in Wasserleitungsrohren, Académie impériale des sciences, 1900.

[12] D. J. Korteweg, „Ueber die Fortpflanzungsgeschwindigkeit des Schalles in elastischen Röhren,“ *Annalen der Physik,* Bd. 241, p. 525–542, 1878.

[13] E. B. Wylie und V. L. Streeter, „Fluid transients,“ *New York,* 1978.

[14] A. Bergant, A. R. Simpson und A. S. Tijsseling, „Water hammer with column separation: A historical review,“ *Journal of Fluids and Structures,* Bd. 22, pp. 135-171, 2006.

[15] E. B. Wylie, V. L. Streeter und L. Suo, Fluid transients in systems, Bd. 1, Prentice Hall Englewood Cliffs, NJ, 1993.

[16] H.-M. Prasser, J. Zschau und A. Böttger, „Entwicklung von Zweiphasenmesstechnik für vergleichende Untersuchungen zur Beschreibung von transienten Strömungen in Rohrleitungen,“ *Abschlussbericht zum BMBF-Vorhaben Nr. 11ZF9504/1,* August 1998.

[17] P. S. Wilson und R. A. Roy, „An audible demonstration of the speed of sound in bubbly liquids,“ *American Journal of Physics,* Bd. 76, p. 975–981, 2008.

[18] C. Zhao und Z. Zhang, „Dynamic Error Correction of Filament Thermocouples with Different Structures of Junction based on Inverse Filtering Method,“ *Micromachines,* Bd. 11, p. 44, 2020.

[19] C. Bombardieri, „Experimental Investigation of the Filling Process in Evacuated Spacecraft Propulsion System Feedlines,“ 2018.

[20] C. Bombardieri, T. Traudt und C. Manfletti, „Experimental and numerical analysis of water hammer during the filling process of pipelines,“ in *Space Propulsion Conference, Cologne, Germany,* 2014.